

Ideal Weyl nodal ring with large drumhead surface state in orthorhombic compound TiS_2

Tie Yang^{1,2,†}, Shoubing Ding^{2,†}, Ying Liu^{3,†}, Zhimin Wu^{2,*} and Gang Zhang^{4,*}

¹ School of Physical Science and Technology, Southwest University, Chongqing 400715, China.

² School of Physics and Electronic Engineering, Chongqing Normal University, Chongqing 401331, China.

³ School of Materials Science and Engineering, Hebei University of Technology, Tianjin 300130, China.

⁴ Institute of High Performance Computing, Agency for Science, Technology and Research, Connexis, 138632, Singapore.

† Authors contributed equally to this work

* Emails: zmwu@cqu.edu.cn and zhangg@ihpc.a-star.edu.sg

Supplementary materials

The ab initio molecular dynamics simulations have been performed on TiS_2 material with a $2 \times 2 \times 2$ supercell for 6000 femtosecond at 300K, 500K and 1000K, and the results of the energy variation and temperature fluctuation are shown in Figure S1. We can find that the TiS_2 structure maintains thermodynamically stable within the whole simulation timescale for the three temperatures since their energy and temperature values exhibit relatively small vibration. In addition, it is also observed that the variation amplitudes increase with temperature raising for both temperature and energy vibrations.

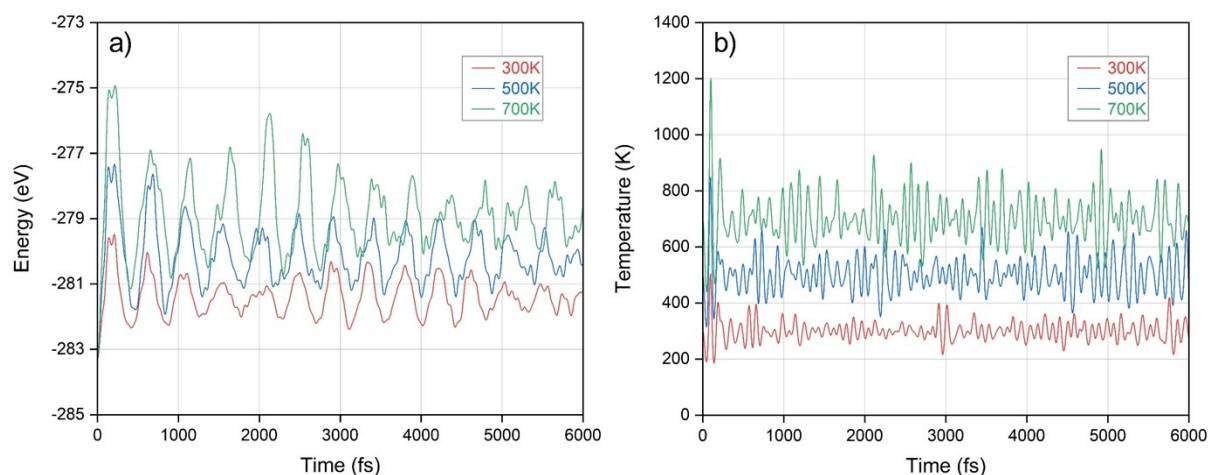


Figure S1: The ab initio molecular dynamics simulation results of energy variation a) and temperature fluctuation b) on TiS_2 material with $2 \times 2 \times 2$ supercell for 6000 femtosecond at 300K, 500K and 1000K.

In order to verify the band structure of TiS_2 material, we further employ the modified Becke-Johnson (MBJ) potential, which has been proved to show favorable accuracy as the

more expensive hybrid functional, and the obtained results are displayed in Figure S2. It can be seen that the two different methods exhibit similar band structure, especially for the band crossing features of the focal point in current study.

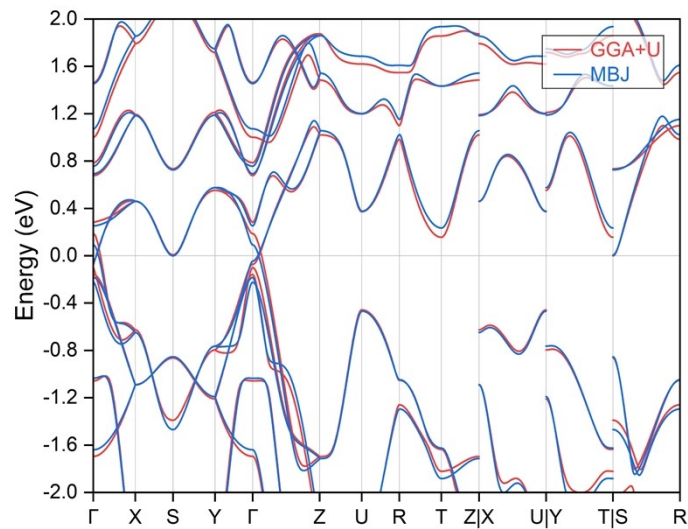


Figure S2: The calculated electronic band structures for TiS_2 material with GGA+U method and MBJ functional.

The specific orbital component decomposition for the band crossing has also been detailed, as plotted in Figure S3 and S4 for S and Ti atoms. Only the different orbital projections of d electrons have been displayed for Ti atoms because the others can be neglected. We can see that the two crossing bands mainly have the p_x and d_{z^2} orbital characters from S and Ti element, respectively.

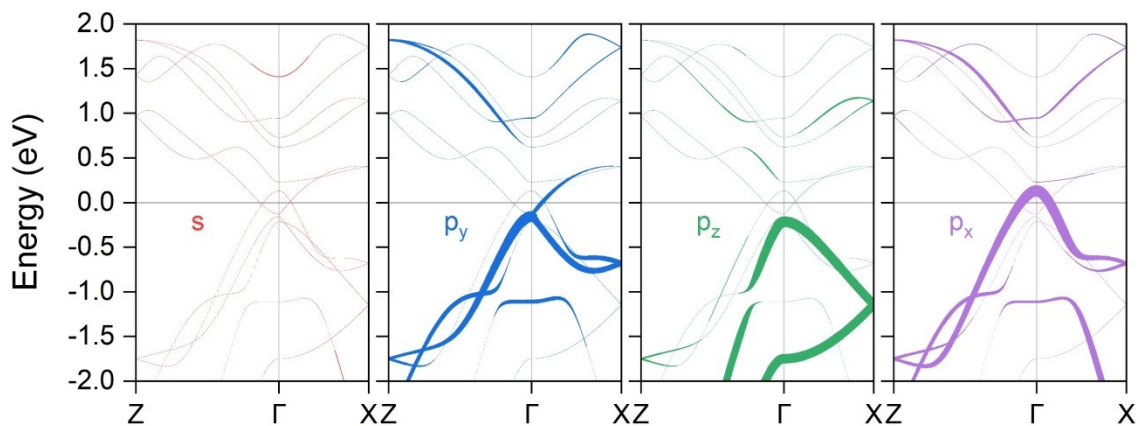


Figure S3: The band crossing areas of TiS_2 material with orbital projection for S atoms.

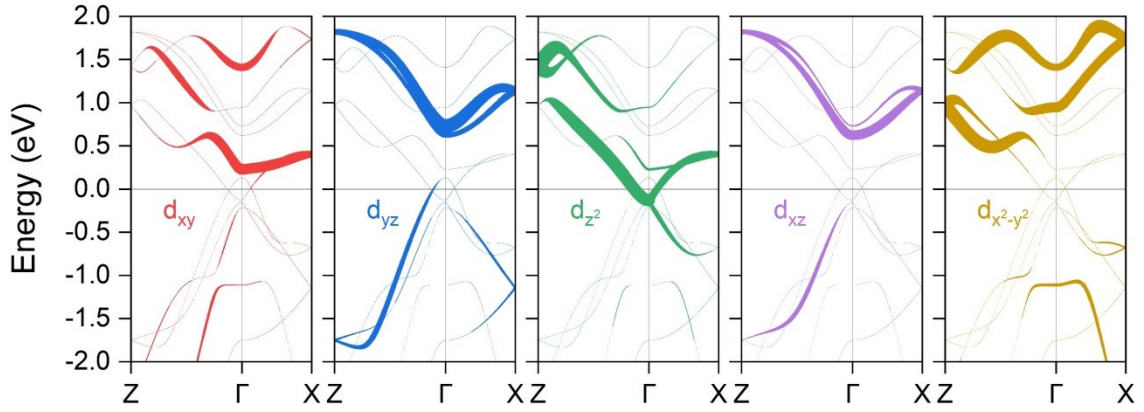


Figure S4: The band crossing areas of TiS_2 material with orbital projection for Ti atoms.

As the relatives of TiS_2 , we have also examined the corresponding properties for TiSe_2 , TiTe_2 , and the obtained results are shown in the following figures. They both exhibit thermodynamic and mechanical stabilities, and moreover, their electronic band structure show similar topological nodal ring states.

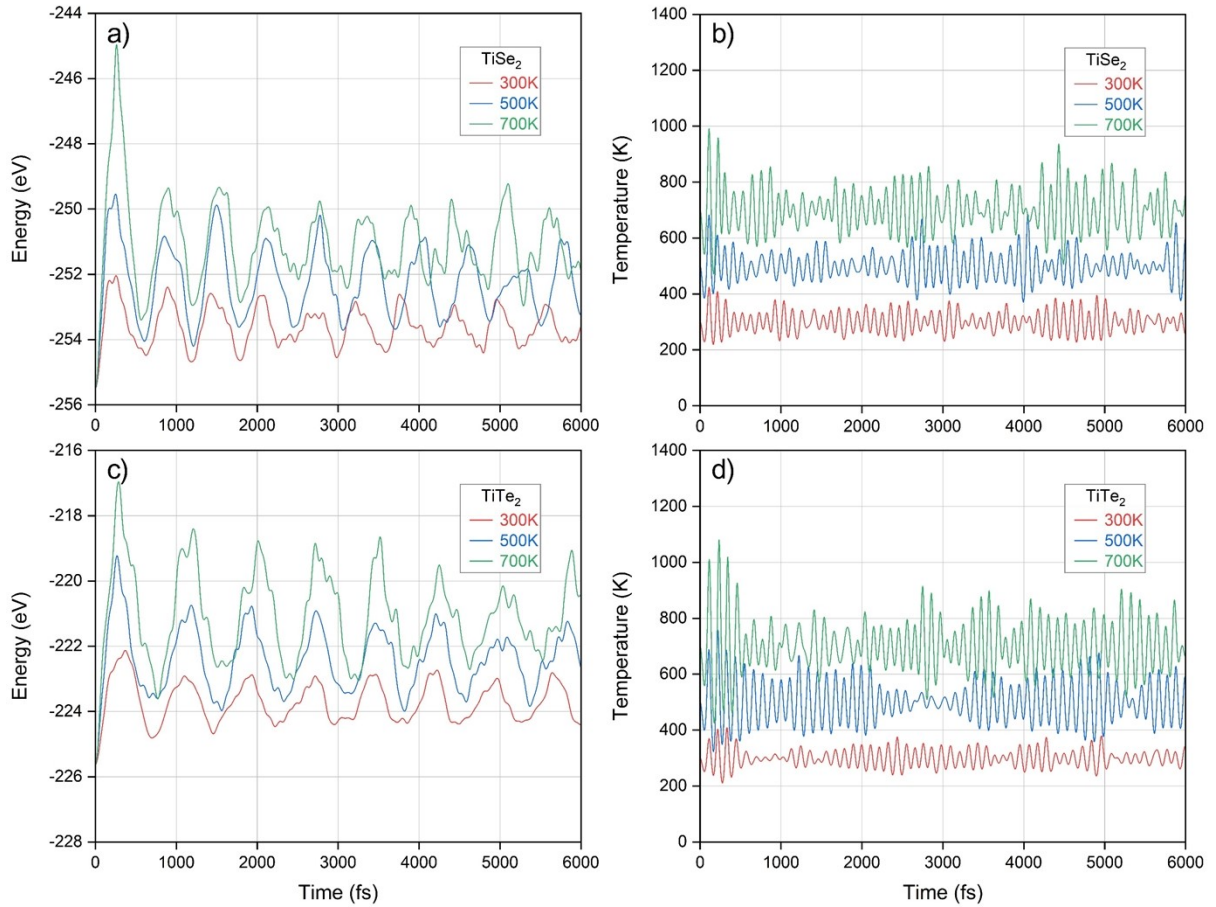


Figure S5: The ab initio molecular dynamics simulation results of energy variation and temperature fluctuation on TiSe_2 and TiTe_2 with $2 \times 2 \times 2$ supercell for 6000 femtosecond at 300K, 500K and 1000K.

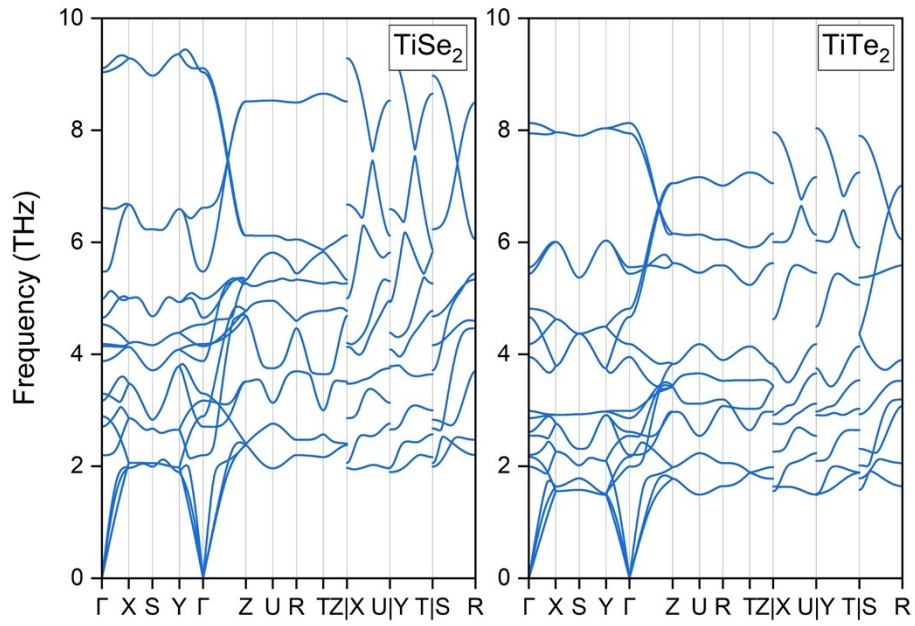


Figure S6: The phonon dispersion spectrum for TiSe_2 and TiTe_2 materials.

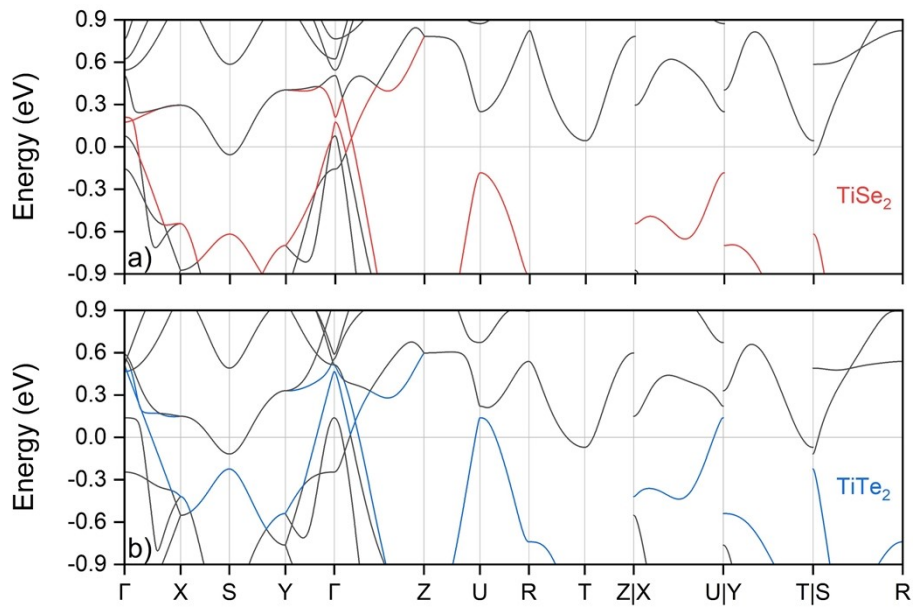


Figure S7: The calculated electronic band structures for TiSe_2 and TiTe_2 materials.

Table S1: The calculated various elastic constants (C_{ij}), Young's modulus E , shear modulus G and Poisson's ratio ν for TiS_2 , TiSe_2 and TiTe_2 . All units are in GPa, except no unit for ν .

Material	C_{11}	C_{12}	C_{13}	C_{22}	C_{23}	C_{33}	C_{44}	C_{55}	C_{66}	E	G	ν
TiS_2	71.9	53.7	52.4	114.8	54.6	151.2	77.9	30.1	72.3	103.4	41.3	0.252
TiSe_2	67.1	30.9	26.2	120.6	36.6	97.5	64.5	40.4	36.5	93.4	39.2	0.192
TiTe_2	80.1	31.2	30.7	105.0	28.8	57.5	50.6	31.4	31.1	75.8	30.9	0.224